minerals

MDPI

Article

Relationships between Alluvial Facies/Depositional Environments, Detrital Zircon U-Pb Geochronology, and Bulk-Rock Geochemistry in the Cretaceous Neungju Basin (Southwest Korea)

Hyojong Lee [1], Min Gyu Kwon [1], Seungwon Shin [2], Hyeongseong Cho [3], Jong-Sun Kim [4], Yul Roh [5], Min Huh [5] and Taejin Choi [1,*]

1 Department of Energy and Resources Engineering, Chosun University, Gwangju 61452, Korea; barefox@gmail.com (H.L.); kmalsrb@naver.com (M.G.K.)
2 Geological Research Center, Geology Division, KIGAM, Daejeon 34132, Korea; ssw7304@kigam.re.kr
3 Department of Geology, Gyeongsang National University, Jinju 52828, Korea; choh@gnu.ac.kr
4 Ecological Survey Division, National Park Research Institute, Korea National Park Service, Wonju 26466, Korea; kjsun@pusan.ac.kr
5 Faculty of Earth Systems and Environmental Sciences, Chonnam University, Gwangju 61186, Korea; rohy@jnu.ac.kr (Y.R.); minhuh@jnu.ac.kr (M.H.)
* Correspondence: tchoi@chosun.ac.kr

Received: 3 September 2020; Accepted: 16 November 2020; Published: 17 November 2020

Abstract: Zircon U-Pb geochronology and bulk-rock geochemistry analyses were carried out to investigate their relationship with depositional environments of the non-marine Neungju Basin sediments in South Korea. The Neungju Basin was formed in an active continental margin setting during the Late Cretaceous with associated volcanism. Detrital zircon age distributions of the Neungju Basin reveal that the source rocks surrounding the basin supplied sediments into the basin from all directions, making different zircon age populations according to the depositional environments. Mudstone geochemistry with support of detrital zircon U-Pb age data reveals how the heterogeneity affects the geochemical characteristics of tectonic setting and weathering intensity. The sediments in the proximal (alluvial fan to sandflat) and distal (playa lake) environments differ compositionally because sediment mixing occurred exclusively in the distal environment. The proximal deposits show a passive margin signature, reflecting their derivation from the adjacent metamorphic and granitic basement rocks. The distal deposits properly indicate an active continental margin setting due to the additional supply of reworked volcaniclastic sediments. The proximal deposits indicate a minor degree of chemical weathering corresponding to fossil and sedimentological records of the basin, whereas the distal deposits show lower weathering intensity by reworking of unaltered volcaniclastic detritus from unstable volcanic and volcaniclastic terranes. Overall, this study highlights that compositional data obtained from a specific location and depositional environments may not describe the overall characteristic of the basin.

Keywords: provenance; compositional heterogeneity; major element; detrital zircon; nonmarine basin

1. Introduction

Geochemical analyses on sediments have been performed to reconstruct the depositional history of sedimentary basins (e.g., [1–5]). The composition of basin fills provides information about the type of source rocks, tectonic settings of the basin, and weathering conditions in the source areas [6–9]. However, sediments originated from different source rocks are progressively mixed during downstream

transportation, generating a compositional contrast between the proximal and distal deposits [10,11]. In the proximal environments close to the basin margins, sediments tend to be deposited separately according to drainage systems, having a wide range of compositional variations. On the other hand, in the distal environments of a basin, sediments may be homogenized by the sediment mixing, having the average composition of surrounding source rocks.

Various tectonic setting discrimination methods and weathering indices have been proposed using the major element composition of sediments and sedimentary rocks. For example, the SiO_2–K_2O/Na_2O and K_2O/Na_2O–SiO_2/Al_2O_3 binary plots by Roser and Korsch [7] have been most widely applied to many provenance studies to discriminate tectonic settings (e.g., [12,13]). In the case of weathering indices, the hemical index of alteration (CIA), defined as molecular $[Al_2O_3/(Al_2O_3 + CaO + Na_2O + K_2O)] \times 100$ [8], has been successfully adopted for more than thirty years (e.g., [14,15]). Previous studies have indicated that these methods may provide inaccurate information due to the statistical limitations of the original dataset, the grain-size effect, and hydraulic sorting [16–18]. However, the influence of the compositional contrast between the proximal and distal deposits on the signatures of tectonic settings and weathering has yet to be tested in a nonmarine basin.

The Cretaceous Neungju Basin, an extensional basin located in the southwestern Korean Peninsula, is an excellent sample site for this study. The Neungju Basin is surrounded by source rocks of various lithology with different formation ages (Figure 1; [19–25]), possibly generating a compositional heterogeneity for the basin fills. Information about depositional environments and sediment transportation has been well constrained by previous studies [26]. Hence, in this study, we aim (1) to investigate variations of the source rocks of the Cretaceous Neungju Basin based on detrital zircon U-Pb ages and (2) to investigate how the compositional heterogeneity of sediments under different depositional environments influence geochemical signatures such as tectonic setting and weathering signatures.

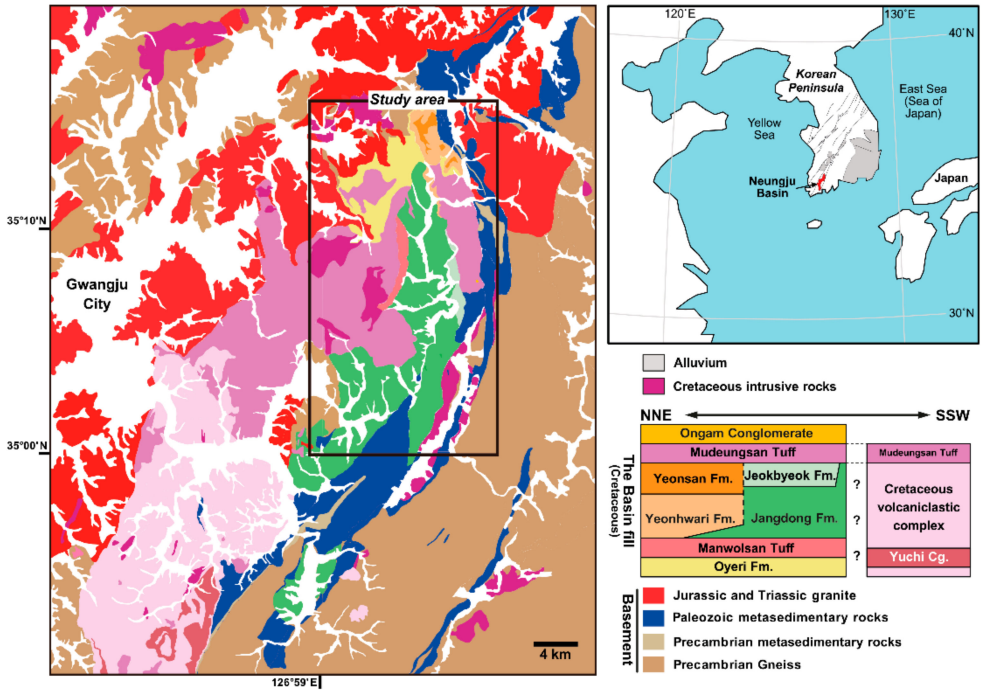

Figure 1. Geological map and stratigraphy of the Neungju Basin (modified after [19–25]). Precambrian granitic gneiss complexes broadly surround the basin. Paleozoic metasedimentary rocks are narrowly distributed along the eastern and southeastern basin margins. Triassic to Jurassic granites are mostly distributed on the northern and western side of the basin. In contrast to the northern part of the basin where epiclastic sediments were mainly deposited, the southern part of the basin was filled with volcaniclastic deposits, forming a volcaniclastic terrane.

2. Geological Settings

During the Cretaceous, NE-SW-trending sinistral strike-slip fault systems were developed along the East Asian continental margin due to oblique subduction of the Izanagi Plate beneath the East Asian continent [27]. Small nonmarine basins were formed under extensional or transtensional tectonic regimes along the NE-SW-trending fault systems in the southern part of the Korean Peninsula [28]. Subduction-related magmatic activity was initiated in central China and migrated eastward to Korea due to the oblique consumption of the ridge [29]. The Cretaceous nonmarine basins were filled with epiclastic and volcaniclastic deposits during extensional faulting and felsic to intermediate volcanic activity.

The Neungju Basin is one of the Cretaceous nonmarine strike-slip basins, located east of Gwangju City (Figure 1). The eastern and western basin margins are bounded by NNE-SSW-trending fault systems. However, the basin margins are unclear because a majority of the margins have been covered by volcaniclastic deposits and volcanic rocks supplied by eruptions during the late-stages of basin development (87–85 Ma; [30]). The basement rocks surrounding the Neungju Basin are mainly composed of three types: (1) Precambrian granitic gneiss complexes, (2) Paleozoic metasedimentary rocks, and (3) Jurassic and Triassic granites (Figure 1). A Precambrian granitic gneiss complex (1935 Ma; [31]) is broadly distributed on the eastern side of the basin, and is also found in areas over the western margin. Paleozoic metasedimentary rocks are narrowly distributed as an elongated belt along the eastern to southeastern basin margins. They are composed of quartzites, carbonates, schists, and coal-bearing shales. Although the depositional ages of the Paleozoic rocks are not clearly constrained, they are considered to be equivalent to the Upper Paleozoic sedimentary succession of Korea (Pyeongan Supergroup; [32]). The Precambrian and Paleozoic rocks have been intruded by Triassic to Jurassic granites (219–176 Ma; [31]).

The Neungju Basin is filled with an approximately 2000 m thick succession of epiclastic and volcaniclastic deposits. The northern part of the basin is mainly filled with epiclastic deposits, occasionally intercalated with volcaniclastic deposits (Figure 1; [20,22]). Whereas, the southern part of the basin is mainly filled with rhyolites, dacitic tuffs, and tuff breccias, subordinately with conglomerates, indicating development of volcaniclastic terrane on the southern part of the basin (Figure 1; [19,23]).

Sedimentological studies on the Neungju Basin have been focused on the northern part (e.g., [26,33,34]). In the northern part of the basin, alluvial fans were developed on the areas proximal to the basin margins, and transitioned to the alluvial plain to sandflat and to the central playa lake (Figure 2; [26]). Paleocurrent data indicate that the sediments derived from the surrounding highlands were transported toward the central playa lake [26]. Reworked volcaniclastic deposits were also supplied to the central playa lake through the alluvial plain and sandflat environments from the southern volcaniclastic terrane [26]. Volcanic activity occasionally intensified during basin development, resulting in the deposition of amalgamated tuff beds tens to hundreds of meters thick (the Manwolsan Tuff, middle Jangdong Tuff, and Mudeungsan Tuff) in the northern part of the basin (Figure 2; [26]).

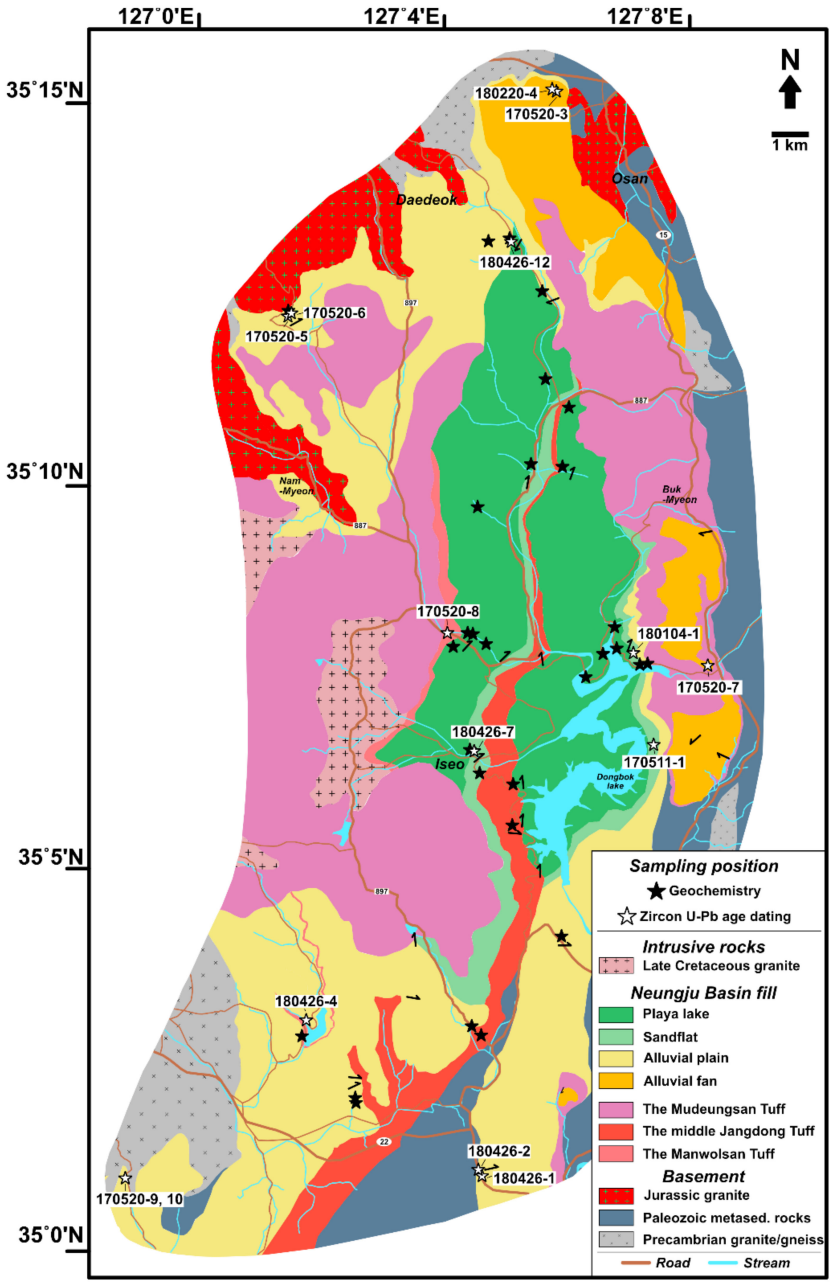

Figure 2. Spatial distribution of depositional environments in present outcrops of the Neungju Basin (modified after [26]). Sixteen mudstone samples were collected from the proximal depositional environments (alluvial plain and sandflat), and fourteen mudstone samples from the distal environment (playa lake). Samples were also collected from conglomerate, sandstone, and tuff and analyzed in terms of zircon U-Pb geochronology to constrain sediment provenance and the depositional age of the basin. Sampling positions for geochemical analysis and zircon U-Pb dating are indicated by closed and open stars, respectively. Black arrows indicate paleocurrent direction [26].

3. Sampling and Analytic Methods

Fifteen conglomerate, sandstone, and tuff samples were collected in the northern part of the Neungju Basin and were subsequently used for zircon U-Pb analysis (Figures 2 and 3). Zircon grains were separated from the collected samples by the conventional heavy mineral separation method. The zircon grains were mounted and polished to expose their cross-sections. Then, scanning-electron-microscope cathodoluminescence (SEM-CL) images of the zircon grains were obtained to identify their internal

structures (Figure 4). Zircon U-Pb isotopic ratios were determined using a Nu Plasma II Multi Collector Inductively Coupled Plasma Mass Spectrometer (Nu Instruments, Wrexham, UK) equipped with a 193 nm ArF excimer Laser Ablation system (New Wave Research, Fremont, CA, USA) (LA-MC-ICPMS) at the Korea Basic Science Institute (KBSI). The Nu Plasma II mass spectrometer contains fixed collectors of sixteen Faraday detectors and five ion-counting electron multipliers. The collectors were arrayed to detect U-Pb isotopic ratios simultaneously as follows: ^{202}Hg (IC 4), ^{204}(Hg + Pb) (IC 3), ^{206}Pb (IC 2), ^{207}Pb (IC 1), ^{208}Pb (IC 0), ^{232}Th (high 7), and ^{238}U (high 9). ^{235}U was calculated from the signal at mass 238 using a natural ratio between ^{238}U/^{235}U = 137.88.

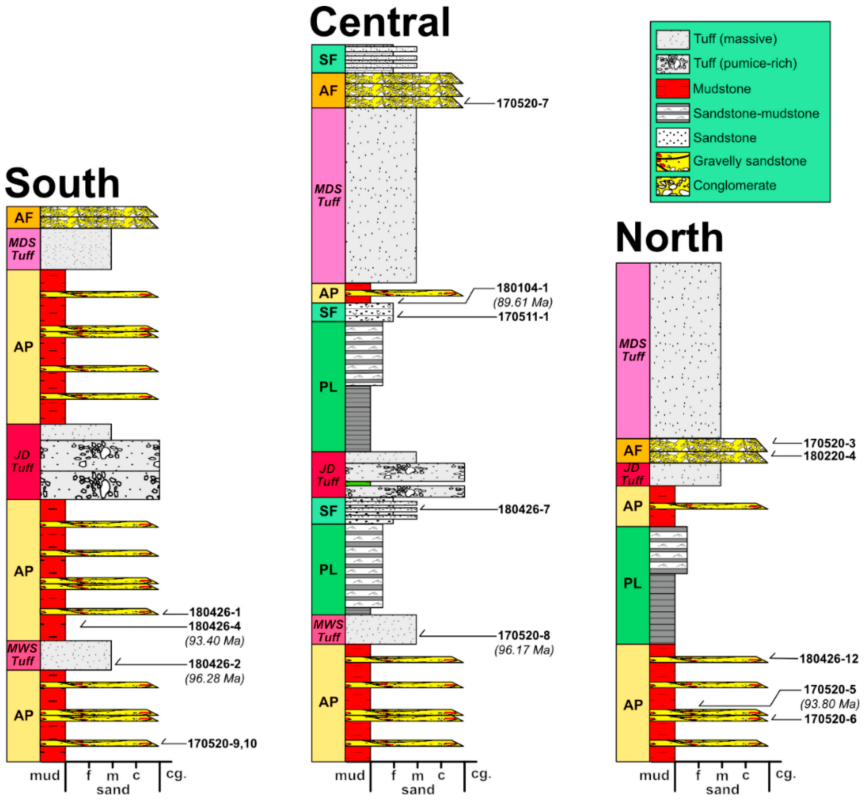

Figure 3. Schematic composite section of the study area (modified from [26]). AF = alluvial fan; AP = alluvial plain; SF = sandflat; PL = playa lake. The amalgamated tuff beds of tens to hundreds of meters thick is represented by MWS tuff = the Manwolsan Tuff; JD Tuff = the middle Jangdong Tuff; MDS Tuff = the Mudeungsan Tuff. Sample locations of the zircon U-Pb analyses are marked.

A mass number of 204 was used as a monitor for common ^{204}Pb after discarding the ^{204}Hg background. All analyses were carried out with a spot size of 15 μm in diameter, a 5 Hz repetition rate, and with an energy density of 3 J/cm^2 using He (650 mL/min.) as the carrier gas. Background intensities, dwell time, and wash out time were measured 30 s, 30 s, and 20 s, respectively. A Time-Resolved Analytical procedure was employed to monitor the measured isotope ratios. Signal intensities for each collector were collected every 0.2 s (integration time). Raw data were corrected for background noise, laser-induced elemental fractionation, mass discrimination, and drift in ion counter gains. U-Pb isotope ratios were calibrated against concordant reference zircons 91500 (1065 Ma; [35]). The reference zircon was measured at the beginning and end of each analytical session and at regular intervals during a session, using protocols adapted from Andersen et al. (2002) [36]. A correlation of signal vs. time was also assumed for the reference zircons. All ages were calculated with 2σ errors, and data reduction was conducted using Iolite 2.5 software package [37,38] and Isoplot 3.71 [39]. Because Mesozoic zircon grains occasionally show inaccurate ^{207}Pb/^{206}Pb ages, ^{206}Pb/^{238}U ages for <1000 Ma and ^{207}Pb/^{206}Pb ages for >1000 Ma were used for age probability curves, with a discordance of <±10%. The discordance

(%) was calculated in two ways: [%discordance = 100*(1 − (^{206}Pb/^{238}U age/^{207}Pb/^{235}U age))] for ^{206}Pb/^{238}U ages < 1000 Ma, [%discordance = 100*(1 − (^{206}Pb/^{238}U age/^{207}Pb/^{206}Pb age))] for ^{206}Pb/^{238}U ages > 1000 Ma.

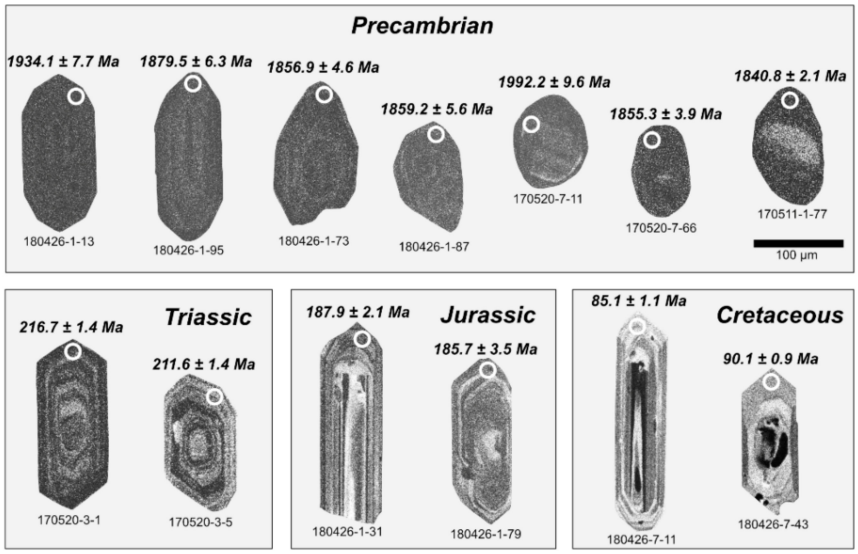

Figure 4. Scanning-electron-microscope (SEM) cathodoluminescence images of the selected zircon grains from the Neungju Basin. Mesozoic zircon grains are characterized by euhedral prismatic shapes, whereas Precambrian zircons tend to show more rounded shapes.

A total of 30 mudstone samples were collected from the proximal and distal deposits in the northern part of the Neungju Basin to investigate compositional contrast in tectonic setting and weathering signatures (Figure 2). Sixteen mudstone samples were collected from the proximal deposits representing alluvial plain (13) and sandflat (3) environments, and 14 mudstone samples were collected from the distal deposits representing the playa lake environment. The collected mudstone samples were powdered in agate mortar after they were washed with clean water and dried. The major element composition of the powdered samples was analyzed at KBSI. A PW2404 X-ray fluorescence spectrometer (XRF, Phillips, Andover, MA, USA) was used on fused glass beads to obtain major element contents, including SiO_2, Al_2O_3, Fe_2O_3 (total Fe), TiO_2, MnO, MgO, K_2O, Na_2O, and P_2O_4. Loss-on-ignition was estimated at 1000 °C for 60 min. The analytic uncertainty is less than 5% for the major element composition.

4. Results

4.1. Detrital Zircon U-Pb Ages

We obtained 1342 concordant (discordance < ± 10%) U-Pb ages from 15 sandstone, conglomerate, and tuff samples ranging from 85.1 ± 1.1 Ma to 3308 ± 3.5 Ma (Table S1). Most of the zircon ages in the conglomerates and sandstones fell into four dominant age groups: Cretaceous (12%; 100–85 Ma), Jurassic (33%; 200–162 Ma), Triassic (10%; 251–202 Ma), and Paleoproterozoic (43%; 2479–1742 Ma). 15 zircons exhibit Archean ages (1.6%; 3308–2510 Ma). A single zircon grain provided a Carboniferous age of 309 ± 17 Ma. The Cretaceous to Triassic zircons are characterized by euhedral prismatic shapes with oscillatory or patchy zonings in their CL images, suggesting a magmatic origin. In contrast, Precambrian zircons show dark and undulatory CL images and their shapes range from euhedral crystal to rounded grains reflecting abrasion during recycling processes (Figure 4). The age distribution of the sandstone samples is presented in the form of a probability density plots (Figure 5; [39]). U-Pb concordia diagrams of the tuffs in the Neungju Basin are shown in Figure 6, while those of the conglomerates and sandstones are shown as supplementary figures (Figures S1 and Figure S2).

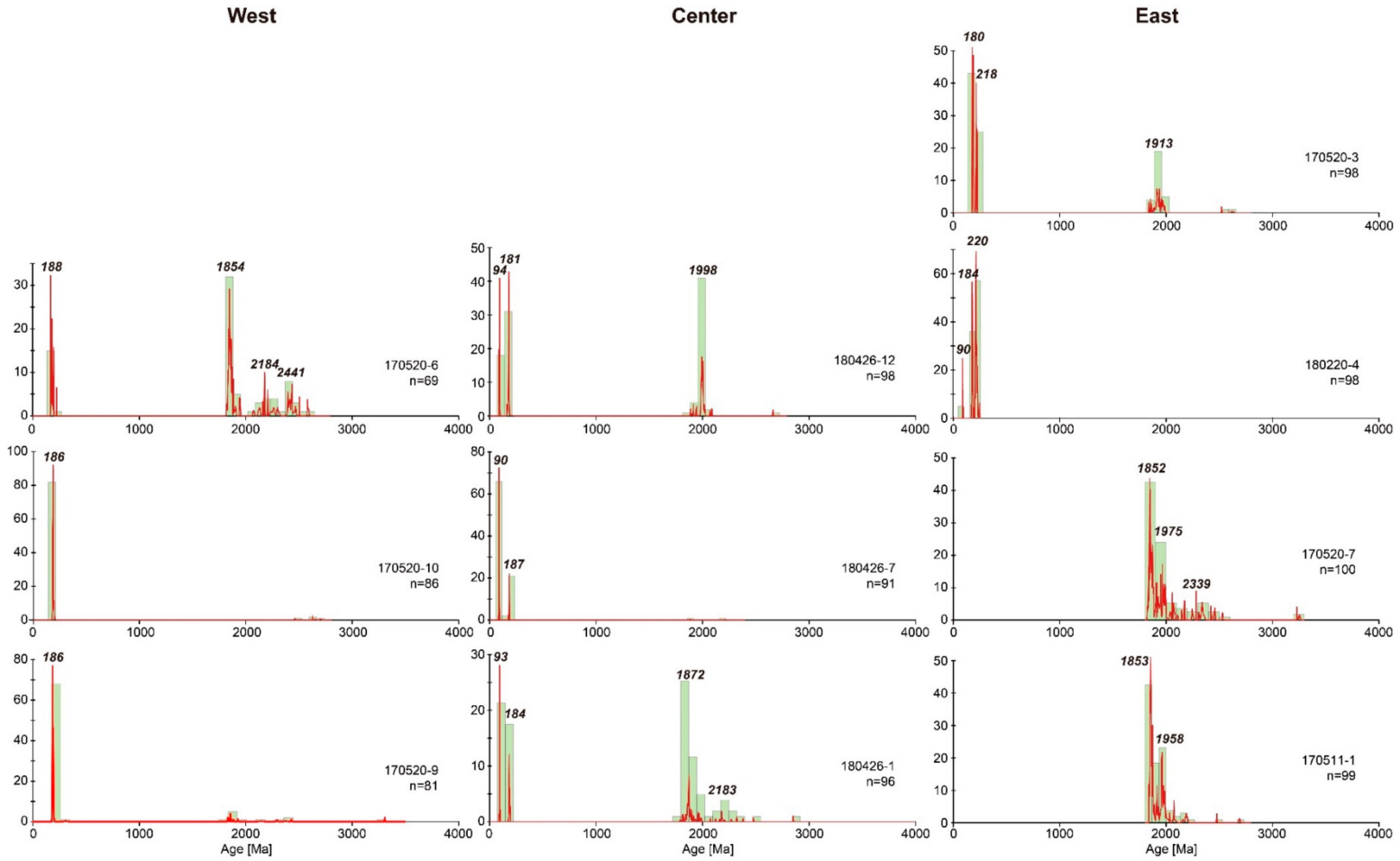

Figure 5. Probability density plots [39] of the detrital zircon grains in the conglomerate and sandstone samples in the Neungju Basin. $^{206}Pb/^{238}U$ ages for <1000 Ma and $^{207}Pb/^{206}Pb$ ages for >1000 Ma were used for age probability curves, with a discordance of <±10%. The plots show differences in their age population according to the sample location. Note that only the age spectra of the central samples and one eastern sample (180220-4) include Cretaceous ages.

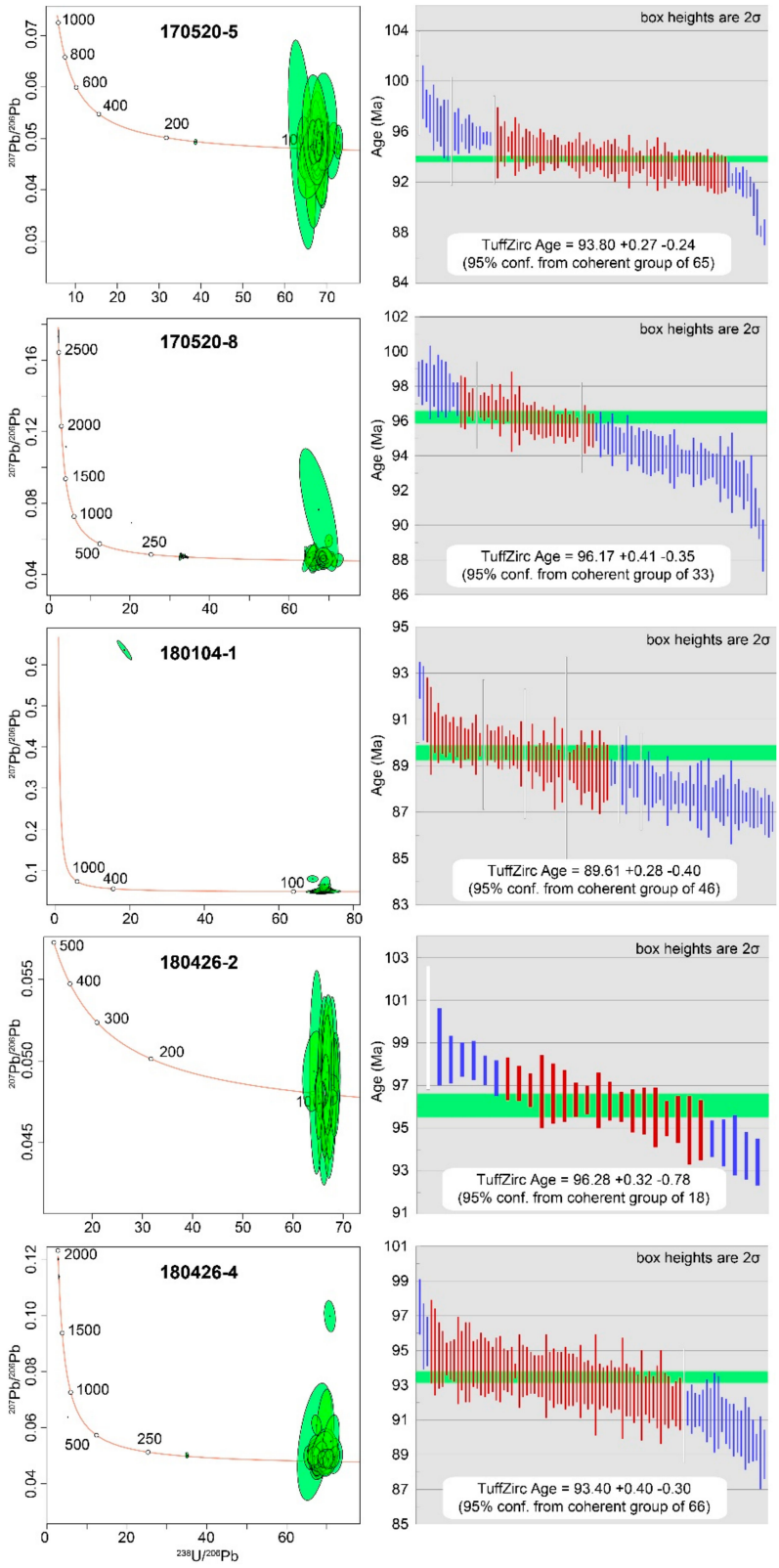

Figure 6. U-Pb Concordia diagrams and weighted mean ages [39] for zircons from tuff samples of the Neungju Basin. Errors are shown at 2-sigma level.

The detrital zircon age populations of the Neungju Basin sediments show variation according to the sample locations (Figures 2–4). The samples near the western and eastern margins have prominent

zircon age peaks indicating their derivation from the adjacent basement rocks. In the northwestern part of the study area, sample 170520-6 showed Jurassic to Triassic ages between 173 and 228 Ma with an age peak at 188 Ma, and Paleoproterozoic to Archean ages between 1830 and 2596 Ma with major age peaks at 1854, 2184, and 2441 Ma. The southwestern samples (170520-9 and 170520-10) are exclusively comprised of Jurassic zircons (peaks at 186 Ma) with no Cretaceous but minor Paleoproterozoic grains. In the northeastern part of the basin, the zircon ages of sample 170520-3 mainly consist of Jurassic to Triassic ages between 178 and 226 Ma with an age peak at 180 and 218 Ma and Paleoproterozoic to Archean ages between 1939 and 2620 Ma with an age peak at 1913 Ma. Sample 180220-4 contains Cretaceous zircon grains between 89 and 99 Ma (5 grains), Jurassic to Triassic zircons between 172 and 251 Ma with prominent age peaks at 220 Ma. In the eastern part of the basin, the zircon age spectra of samples 170511-1 and 170520-7 comprise exclusively of Paleoproterozoic zircons with minor Archean. Sample 170511-1 has zircon grains mainly formed in 1905–2690 Ma with age peaks at 1853 and 1958 Ma. The zircon ages of sample 170520-7 consist of Paleoproterozoic zircons between 1846 and 3254 Ma with prominent age peaks at 1852, 1975, and 2339 Ma.

The basin-fill in the central part of the study area is characterized by significant amounts of zircons from the Late Cretaceous. The zircons of the northernmost sample (180426-12) include three main age groups: Late Cretaceous (95–88 Ma), Jurassic (186–162 Ma), and Paleoproterozoic to Archean (2663–1998 Ma) with age peaks at 94 Ma, 181 Ma and, 1998 Ma, respectively. Sample 180426-7 has zircon age populations of Cretaceous ages between 85 and 94 Ma with a prominent age peak at 90 Ma, Jurassic ages between 178 and 191 Ma with an age peak at 187 Ma, minor Paleoproterozoic ages between 1899 and 2215 Ma. The south sample (180426-1) shows zircon ages of Cretaceous (100–88 Ma) with an age peak at 93 Ma, Jurassic ages (193–179 Ma) with an age peak at 184 Ma, and Paleoproterozoic to Archean ages between 1742 and 2855 Ma with age peaks at 1872 and 2183 Ma.

The tuff samples (170520-5, 170520-8, 180426-2, 180426-4, and 180104-1) show their weighted mean ages as ca. 93.80 Ma, 96.17 Ma, 96.28 Ma, 93.40 Ma, and 89.61 Ma, respectively (Table S1 and Figure 6). Each sample contains several older zircon grains ranging in age from Late Archean (2593 Ma) to Jurassic (164 Ma). All the tuff samples have different eruption ages, indicative of frequent magmatic activity in the area adjacent to the Neungju Basin during its deposition.

4.2. Major Element Composition of Mudstones

The major element composition of the mudstone samples is presented in Table S2. In comparison to Post-Archean Average Shale (PAAS; [40]), the mudstone samples from the Neungju Basin are generally enriched in SiO_2, K_2O, Na_2O, and CaO, and depleted in MgO, Fe_2O_3, TiO_2, MnO and P_2O_5 (Figure 7). Although the samples show similar compositional characteristics for most of the major element contents regardless of their depositional environments, they are clearly distinguished in terms of the Na_2O content (Figure 8). The proximal deposits from the alluvial plain to sandflat environments show the Na_2O content ranging from 1.07% to 3.40%, with an average of 1.99%. In contrast, the distal deposits from the central playa lake show the Na_2O ranging from 1.35% to 4.95%, with an average of 3.50%. Each sample group show no distinctive compositional variation spatially. As presented in Figure 8, the proximal and distal deposits collected from different locations of the study area show similar ranges of major element composition, respectively.

New discriminant-function-based diagrams by Verma and Armstrong-Altrin (2013) [41] can discriminate tectonic settings of sedimentary rocks to three types: island or continental arc, continental rift, and collision. In this diagram, the proximal deposits are plotted near the boundary between the arc and collision fields (Figure 9c), possibly reflecting their derivation from source rocks, including volcanic rocks, metamorphic and metasedimentary rocks. The distal deposits are not overlapped with the proximal deposits in the diagram, indicating the compositional difference between the two sample groups. The distal deposits are plotted near the boundary between the collision and rift fields (Figure 9c). Source rocks for these samples are likely to be composed of metamorphic and metasedimentary rocks and felsic plutonic rocks.

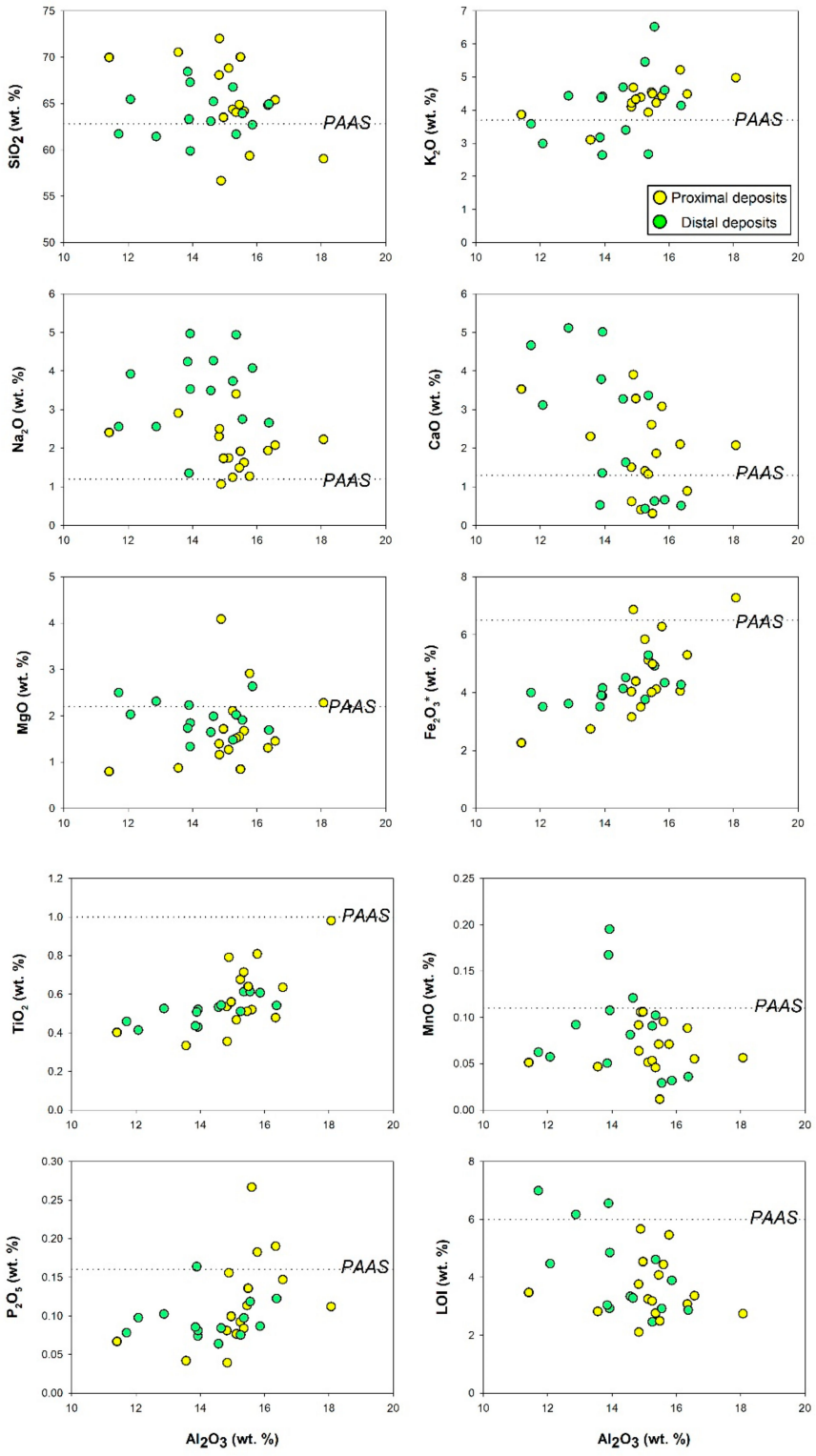

Figure 7. Binary plots of major elements versus Al_2O_3 for the mudstone samples. The proximal and distal deposits are clearly distinguished in terms of the Na_2O content.

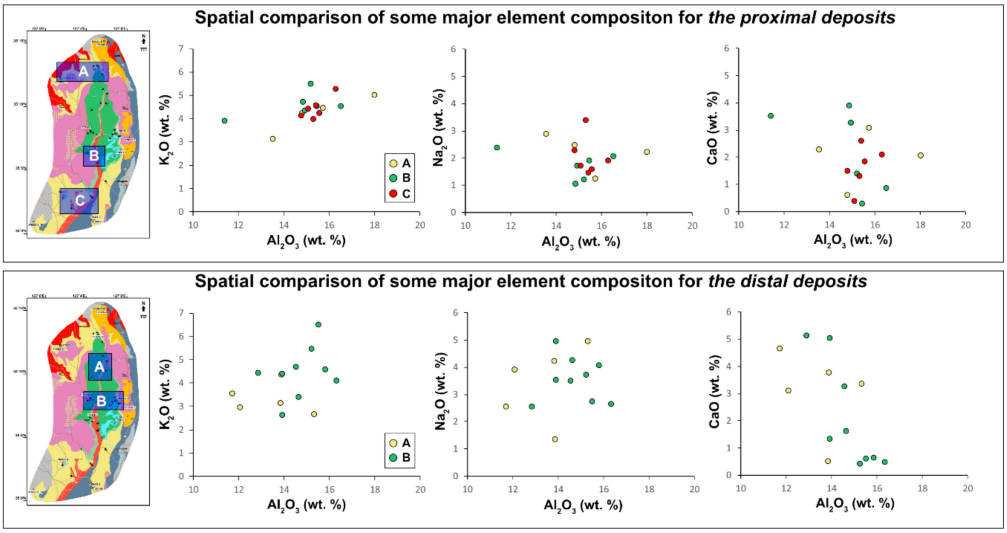

Figure 8. Spatial comparisons of some major element composition for the proximal and distal deposits. Each sample group shows similar range of major element composition, respectively.

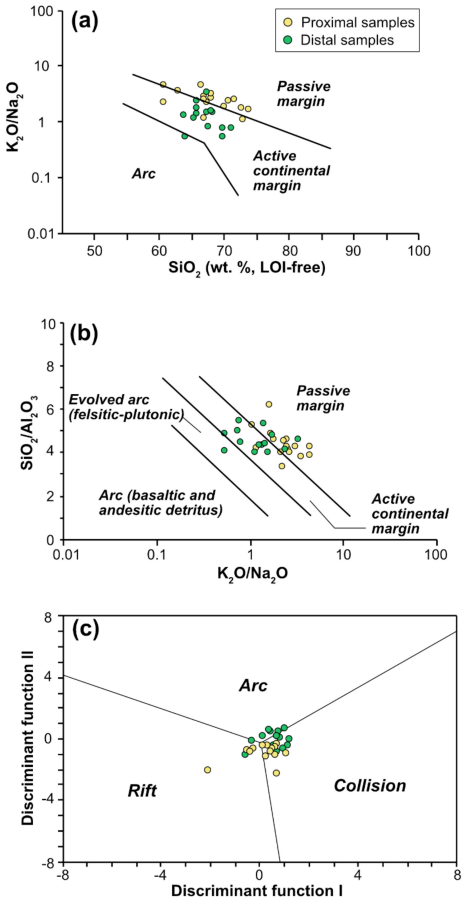

Figure 9. Tectonic setting discrimination diagrams for the mudstone samples. (**a**) K_2O/Na_2O–SiO_2 diagram [7]. (**b**) SiO_2/Al_2O_3–K_2O/Na_2O diagram [7] (**c**) Discriminant function diagram for high-silica [$(SiO_2)_{adj}$ = 63–95%] samples [41], where $(SiO_2)_{adj}$ refers to the modified SiO_2 value after volatile-free recalculation of the major elements to 100%. Two mudstone samples classified as low-silica [$(SiO_2)_{adj}$ = 35–63%] are plotted in the rift field (not presented). The proximal and distal deposits are plotted in these tectonic setting discrimination diagrams separately with minor overlap.

4.3. Weathering Intensities of Mudstones

Various weathering indices have been proposed to assess the degree of chemical weathering quantitatively for sediments and sedimentary rocks. The representative indices for the mudstones in the Neungju Basin are presented in Table 1 and Figure 10.

Table 1. Weathering indices for the mudstone samples from the Neungju Basin.

Depositional Environment	Sample Code	CIA	PIA	CPA	WIP	V	STI
Alluvial plain	180220-1	56	59	88	65	1.37	81.8
Alluvial plain	180426-4	57	61	80	64	1.92	85.1
Alluvial plain	180426-6	63	70	83	64	2.46	83.5
Alluvial plain	180426-12	60	66	78	64	2.37	86.8
Alluvial plain	180426-13	52	53	74	61	1.52	87.4
Alluvial plain	4-26-1050	64	74	84	58	2.92	85.5
Alluvial plain	4-26-1104	59	65	85	60	1.96	84.3
Alluvial plain	180426-11	59	63	83	74	1.78	80.0
Alluvial plain	180427-12-7	56	60	84	71	2.14	84.3
Alluvial plain	4-11-425	56	59	86	63	1.84	84.6
Alluvial plain	4-17-239-r	59	67	88	67	2.13	83.6
Alluvial plain	4-17-239-g	52	53	89	71	1.04	81.8
Alluvial plain	4-46-420	56	58	73	72	1.66	83.3
Sandflat	180426-7	64	74	83	59	3.49	84.5
Sandflat	4-11-1150	44	41	74	66	1.26	87.6
Sandflat	4-17-300	53	54	84	66	1.49	84.3
Playa lake	180426-8	47	47	65	82	0.94	83.5
Playa lake	4-10-239	44	42	65	75	0.89	86.8
Playa lake	4-10-445	41	38	74	73	0.82	86.1
Playa lake	0307-1-905	46	45	72	85	1.24	84.5
Playa lake	1129-1-1	52	52	68	78	1.22	84.8
Playa lake	1129-1-2	51	51	63	75	1.20	86.1
Playa lake	1129-3-2	41	38	71	88	0.96	84.4
Playa lake	180426-9	50	50	86	65	1.26	85.0
Playa lake	180427-14-37	55	60	77	88	2.16	83.8
Playa lake	180427-15-24	54	57	71	86	1.98	84.9
Playa lake	180427-15-39	55	58	70	86	1.43	83.5
Playa lake	4-10-408	55	57	67	72	1.40	86.3
Playa lake	4-11-110	63	69	79	66	2.18	84.0
Playa lake	4-17-340	41	37	75	81	0.91	85.1

The CIA is the most widely used weathering index, monitoring decomposition of feldspar grains and consequent formation of Al-rich clay minerals such as illite and kaolinite [8]. Fresh igneous rocks are found to have a CIA value between 45 and 55, whereas moderately weathered shales such as PAAS yield a value closer to 70 [8]. The CIA values of the mudstone samples range from 44 to 64, with an average of 56, indicating a minor degree of chemical weathering. Although the proximal and distal deposits show some overlap in their CIA values, they can be separated roughly at the CIA value of 54 (Figure 10). The CIA values of the proximal deposits range from 49 to 64, with an average of 59, indicating minor chemical weathering in the source areas. On the other hand, the value of the distal deposits ranges from 44 to 63, with an average of 52, indicating little alterations in the source areas. Weathering indices such as the Plagioclase Index of Alteration (PIA; [42]), the Chemical Proxy of Alteration (CPA; [43]), the Vogt's residual index (V; [44]), and the weathering Index of Parker (WIP; [45]) are also formulated to assess the leaching of mobile elements such as Na_2O, CaO, and MgO during weathering processes. In this study, they provide similar results with those of the CIA value (Figure 9). A low degree of chemical weathering is inferred for the distal deposits, and these samples are distinguished from the more weathered proximal deposits. The Silica–Titania Index (STI; [46]) is the only weathering index that showed a similar degree of chemical weathering for the proximal and

distal deposits. The STI values of the proximal and distal deposits range from 80 to 88 (av. = 84) and 83 to 87 (av. = 85), respectively, indicating a slightly weathered condition [46].

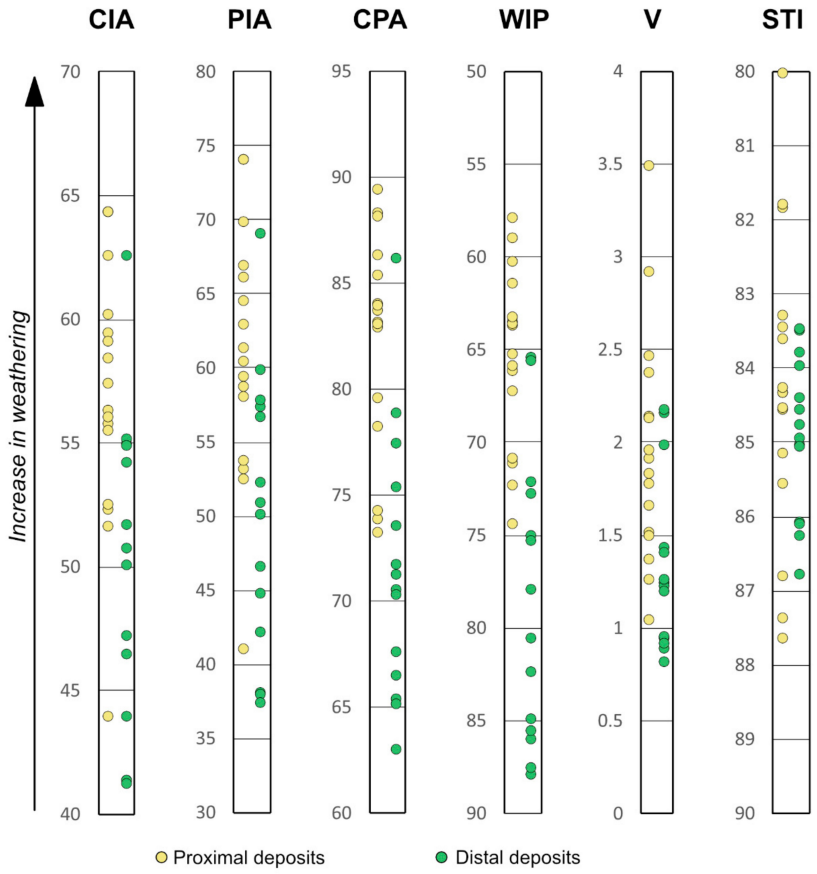

Figure 10. Conventional weathering indices for the mudstone samples. The weathering indices were formulated as molar calculation of some major elements: CIA = [Al_2O_3/(Al_2O_3 + CaO + Na_2O + K_2O)] × 100; PIA = (Al_2O_3 – K_2O)/(Al_2O_3 + CaO + Na_2O – K_2O) × 100; CPA = Al_2O_3/(Al_2O_3 + Na_2O) × 100; WIP = (2Na_2O/0.35 + MgO/0.9 + 2K_2O/0.25 + CaO/0.7) × 100; V = (Al_2O_3+ K_2O)/(MgO + CaO + Na_2O); and STI = (SiO_2/TiO_2)/[(SiO_2/TiO_2) + (SiO_2/Al_2O_3)] + (Al_2O_3/TiO_2)] × 100. In most of the weathering indices, except for the STI index, the distal deposits indicate lower degree of chemical weathering in compared to the proximal deposits.

5. Discussion

5.1. Depositional Age of the Neungju Basin

Our tuff samples show zircon age peaks ranging from ca. 96 to ca. 90 Ma, indicating the depositional age of the Neungju Basin. The sedimentation of the Neungju Basin began before ca. 96 Ma and continued after the Mudeungsan Tuff (Figures 2 and 3) erupted during 87–85 Ma [30]. After the eruption, the deposition occurred in the alluvial fan environment at the limited area in the basin's eastern part.

The frequent alternation of the Late Cretaceous volcaniclastic and epiclastic sediments in the Neungju Basin indicates the tectonic setting of the basin. Arc magmatism prevailed in the southwestern Korean Peninsula during the Late Cretaceous, forming a volcanic complex covering the region [47,48]. Kim et al. (2016) [47] subdivided the Cretaceous igneous rocks in the Korean Peninsula into four groups based on the formation timing: Group I (110–100 Ma), Group II (100–87 Ma), and Group III-IV (86–70 Ma). These groups are also distributed in a NW-SE direction; Group I in the northwest; Group II in the center; Group III-IV in the southeast. Group I-IV suggests the changes in the subduction modes

of the paleo-Pacific Plate (Izanagi Plate) as slab rollback, slab steepening and melting, slab shallowing, and slab rollback and steepening, respectively [47]. The Cretaceous zircons in the Neungju Basin suggest that the basin was deposited during Group II magmatism, formed by inland-ward migrating arc magmatism in the Korean Peninsula.

5.2. Sediment Provenance of the Neungju Basin Based on Detrital Zircon Geochronology

Most detrital zircon grains in the Neungju Basin sandstones and conglomerates have age peaks at the Late Cretaceous (94–90 Ma), Jurassic (188–180 Ma), Triassic (218 Ma), and Paleoproterozoic (2441–1852 Ma) (Figure 5). Zircon ages of the tuff samples (96–90 Ma) in this study indicate that the Late Cretaceous detrital zircon grains in the Neungju Basin were derived from the synsedimentary volcanic or volcaniclastic rocks. Previous studies suggested that the tuff strata of the Neungju Basin derived from the southwest of the basin based on increasing southwestward thickness of the strata [20,22]. The Jurassic and Triassic zircon grains might be derived from the adjacent Mesozoic granites surrounding the basin (Figure 1). The Paleoproterozoic zircons could be supplied from Precambrian metamorphic rocks and Paleozoic metasedimentary rocks surrounding the basin. Most Precambrian metamorphic rocks in the Korean Peninsula formed in ca. 1.9–1.8 Ga [49–51], while the zircon grains older than 1.9 Ga are mainly found as detritus in metasedimentary rocks in Korea [52,53]. In addition, the detrital zircon age distribution of the Paleozoic metasedimentary basement rocks consists of Paleoproterozoic (a peak at ca. 1870 Ma) and Archean ages (a peak at ca. 2490 Ma) with no Paleozoic ages [54]. Hence, the source rocks of the Neungju Basin consists of Late Cretaceous volcanic/volcaniclastic rocks, Jurassic and Triassic granites, Paleozoic metasedimentary rocks, and Precambrian metamorphic rocks.

The detrital zircon U-Pb age data of the Neungju Basin show that sediment detritus in the proximal deposits close to the basin margin derived from nearby basement rocks with no or little Late Cretaceous volcanic material, in spite of their intercalation with Late Cretaceous tuff beds. The samples (170520-7 and 170511-1) near the eastern margin include zircon age clusters of Paleoproterozoic to Archean ages only, suggesting sediment derivation from the Precambrian metamorphic rocks distributed east of the basin. In contrast, the samples collected from the areas near the northeastern (170520-3 and 180220-4) and western margins (170520-6 and 170520-9) show zircon age clusters of Mesozoic ages between Jurassic and Triassic as well as Paleoproterozoic and Archean ages, although sample 180220-4 has five grains of Cretaceous aged zircons. Most of the sediment detritus were supplied from the Jurassic and Triassic granites and Precambrian metamorphic rocks broadly distributed to the north and west of the basin.

In contrast to the sandstone and conglomerate samples collected from the areas close to the basin margins, those collected from the southern and central parts of the study area (180426-1, 180526-7, and 180426-12) show distinct Late Cretaceous peak ages with variable amounts of Jurassic and Paleoproterozoic to Archean ages. A previous sedimentological study in the Neungju Basin reports that a playa lake had been developed in the central parts of the study area [26]. Sediment detritus derived from the respective source rocks were possibly mixed in the central areas of the playa lake and sandflat environments, resulting in more mixed zircon age peaks than those in the samples from proximal areas. The Cretaceous zircons were possibly reworked from the volcaniclastic terrane located at the south of the basin and transported northward to the central playa lake (e.g., [55,56]). Paleocurrent data support the derivation of the Cretaceous zircon grains from the south [26]. Direct derivation of the Cretaceous zircons by syndepositional volcanism is less reliable because tuff beds were not observed in the outcrop sections where the sandstone and conglomerate samples were collected, and their stratigraphic positions correspond to inter-eruption periods of the Neungju Basin [26].

5.3. Contrasting Geochemical Signatures of Tectonic Settings and Weathering Intensities in a Nonmarine Basin

The compositional contrast between the proximal and distal deposits can be explained based on the data collected from zircon age dating. The zircon age data indicate that Jurassic to Triassic granites and Precambrian metamorphic rocks as the primary sources in the marginal areas where

alluvial drainage systems transported sediment detritus from the adjacent source areas. These source rocks have similar characteristics in major element composition [57]. Thus, the proximal deposits show similar major element composition regardless of variations in the relative contribution of Jurassic to Triassic granites and Precambrian metamorphic rocks. In contrast, the zircon age data indicate that considerable amounts of sediments were transported from the southern Cretaceous volcaniclastic terrane to the central playa lake. Cretaceous volcanic activity in the Neungju Basin areas was generated from calk-alkaline magma, resulting in the deposition of felsic pyroclastic, andesitic to dacitic rocks, and rhyolite [58–60]. Although various types of volcanic rocks were formed, they are characterized by abundant plagioclase content. Thus, it would be natural that the distal deposits show high Na_2O content than the proximal deposits.

Differences in weathering conditions in the source areas might have enhanced the compositional contrast between the proximal and distal deposits. Fossil and sedimentological evidence revealed in the Cretaceous Gyeongsang Basin, South Korea, indicated arid to semi-arid conditions in the Korean Peninsula during the Late Cretaceous (e.g., [34,61,62]). Besides, Lee and Lee (2003) [63] reported that the Hayang Group mudstones in the Gyeongsang Basin, correlate with the Neungju Basin fills, resulting in CIA values ranging from 54 to 67, with an average of 61. The CIA values in the Neungju Basin are consistent with the previous results, indicative of the weathering condition under the equilibrium state in the source areas. This results in a minor degree of compositional alteration for the proximal deposits due to loss of the mobile elements (e.g., Na_2O and CaO) during weathering processes. The weathering intensities of the distal deposits, however, are much lower than expected. To assess the weathering intensity properly, chemical loss of the mobile elements and the soil profile's physical erosion should occur at a stable rate in the source areas [64]. Active tectonism and storms may enhance the physical erosion of fresh bedrocks and less altered lower horizons of the soil profile, resulting in a lower estimate of weathering intensities (e.g., [65,66]). In the Neungju Basin, volcaniclastic terrane with high and unstable topography might have been formed in the southern part of the basin in a short time due to intense volcanic activities. After the rapid aggradation of the large volume of volcaniclastic sediments in the volcaniclastic terrane, the unconsolidated volcanic/volcaniclastic materials were easily eroded, reworked, and transported as debris-flows to the central playa lake far from the volcaniclastic terrane during the inter-eruption period (e.g., [67,68]). Thus, sediment detritus originated from the southern volcaniclastic terrane might be difficult to experience compositional alteration due to chemical weathering in the source areas, resulting in the distal deposits' low weathering intensities.

In this study, the differences in source rock composition cause the compositional contrast between the proximal and distal deposits, resulting in different tectonic setting signatures based on their major element composition. The central playa lake in the Neungju Basin acted as a mixing bowl for the sediments derived from various source rocks. In addition to sediments originated from Precambrian gneiss and Mesozoic granites, Na_2O-rich sediments from the southern Cretaceous volcaniclastic terrane were mixed in the playa lake, resulting in the active continental margin signatures for the distal deposits. On the contrary, in the basin's marginal areas, sediment mixing from different source rocks was inhibited. The proximal deposits reflect only the composition of adjacent source rocks, providing inadequate information about the tectonic setting of the basin. The compositional alteration due to chemical weathering might also influence the shift from active continental margin to the passive margin signature in the tectonic setting discrimination diagrams due to the loss of mobile elements. Overall, this study implies that geochemical indicators should be used with caution for nonmarine sediment because of the compositional heterogeneity of the basin-fill. The tectonic setting of a basin can be inferred by the composition of sediments deposited in the distal environments where sediments from various source rocks are mixed.

6. Conclusions

To investigate the compositional contrast of sediments in a nonmarine basin and its influence on the tectonic setting and weathering signatures, the nonmarine Neungju Basin was studied through the

analysis of mudstone geochemistry supported by zircon U-Pb age dating. A total of 1342 zircon age data ranging from 3308 to 85 Ma mainly consists of Cretaceous (100-85 Ma), Jurassic (200–162 Ma), Triassic (251–202 Ma), Paleoproterozoic (2479–1742 Ma), and Archean (3308–2510 Ma). The results show that the evolution of the Neungju Basin was controlled by changes in subduction modes of the Paleo-Pacific Plate.

The Neungju Basin sediment was supplied from four different types of source rocks surrounding the basin; Precambrian metamorphic, Paleozoic metasedimentary, and Cretaceous volcanic rocks, as well as Jurassic and Triassic granites. These source rocks supplied sediments into the basin from all directions, making different zircon age distributions according to the depositional environments. The sediments in the proximal environments (alluvial fan to sandflat) close to the basin margins were derived from the adjacent basement rocks. On the contrary, in the distal environment (the central playa lake), sediments transported from the proximal deposits were mixed.

Mudstones deposited in the proximal deposits reflect the composition of nearby source rocks, whereas mudstones deposited in the distal deposits reflect the mixed characteristics of the source rocks. Due to the exclusive input of volcaniclastic sediment into the distal deposits, tectonic setting signatures differ significantly between the proximal and distal deposits. The proximal deposits show passive margin signatures, reflecting their derivation from metamorphic and granitic rocks, whereas the distal deposits show active continental margin signatures reflecting the overall source rock signatures. In the case of weathering, the proximal deposits indicate slightly higher weathering intensities than the distal deposits. Reworking of fresh volcanic detritus from the southern volcaniclastic terrane might have lowered the weathering intensities of the distal deposits.

Overall, this study implies that compositional analysis for reconstructing tectonic settings and weathering conditions should be carefully performed with support from detailed provenance and paleoenvironmental analyses. A nonmarine basin may have strong spatial contrast in sediment composition due to preferential mixing of source rocks, and a specific location and depositional environment may not reflect the overall characteristics of the basin.

Supplementary Materials: The following are available online at http://www.mdpi.com/2075-163X/10/11/1023/s1, Figure S1: U-Pb Concordia diagrams for zircons from conglomerate and sandstone samples of the Neungju Basin (continued to Figure S2). Errors are shown at 2-sigma level. Figure S2: U-Pb Concordia diagrams for zircons from conglomerate and sandstone samples of the Neungju Basin (continued from Figure S1). Errors are shown at 2-sigma level. Table S1: Zircon U-Pb isotopic ratios of the conglomerate, sandstone, and tuff samples from the Neungju Basin. Table S2: Major element composition of the mudstone samples from the Neungju Basin.

Author Contributions: Conceptualization, H.L. and T.C.; methodology, M.G.K., T.C., and H.L.; investigation, M.G.K., H.L., S.S., and H.C.; writing—original draft preparation, H.L.; writing—review and editing, T.C.; project administration, Y.R. and J.-S.K.; funding acquisition, M.H. Detrital zircon U-Pb age data of this work represents part of M.G.K.'s Masters Research performed at the Chosun University. All authors have read and agreed to the published version of the manuscript.

Funding: This research was funded by the National Research Foundation of Korea (NRF), grant number 2020R111A3072160, research grant from Damyang and Hwasun Counties, Republic of Korea to T.C. The APC was funded by the National Research Foundation of Korea (NRF), grant number 2020R111A3072160.

Acknowledgments: We thank the Editors Wilfried Winkler and Albrecht von Quadt and anonymous journal reviewers for their thoughtful comments.

Conflicts of Interest: The authors declare no conflict of interest. The funders had no role in the design of the study; in the collection, analyses, or interpretation of data; in the writing of the manuscript, or in the decision to publish the results.

References

1. Ohta, T. Geochemistry of Jurassic to earliest Cretaceous deposits in the Nagato Basin, SW Japan: Implication of factor analysis to sorting effects and provenance signatures. *Sediment. Geol.* **2004**, *171*, 159–180. [CrossRef]
2. Yang, J.; Du, Y.; Cawood, P.A.; Xu, Y. Modal and Geochemical Compositions of the Lower Silurian Clastic Rocks In North Qilian, NW China: Implications For Provenance, Chemical Weathering, and Tectonic Setting. *J. Sediment. Res.* **2012**, *82*, 92–103. [CrossRef]

3. Gu, X.X.; Liu, J.M.; Zheng, M.H.; Tang, J.X.; Qi, L. Provenance and tectonic setting of the Proterozoic turbidites in Hunan, South China: Geochemical evidence. *J. Sediment. Res.* **2002**, *72*, 393–407. [CrossRef]
4. Lee, J.I.; Lee, Y.I. Provenance of the lower Cretaceous Hayang Group, Gyeongsang Basin, southeastern Korea: Implications for continental-arc volcanism. *J. Sediment. Res.* **2000**, *70*, 151–158. [CrossRef]
5. Joo, Y.J.; Lee, Y.I.; Hisada, K.I. Provenance of Jurassic accretionary complex: Mino terrane, inner zone of south-west Japan—Implications for palaeogeography of eastern Asia. *Sedimentology* **2007**, *54*, 515–543. [CrossRef]
6. Roser, B.P.; Korsch, R.J. Provenance signatures of sandstone–mudstone suites determined using discriminant function analysis of major element data. *Chem. Geol.* **1988**, *67*, 119–139. [CrossRef]
7. Roser, B.P.; Korsch, R.J. Determination of tectonic settings of sandstone–mudstone suites using SiO_2 content and K_2O/Na_2O ratio. *J. Geol.* **1986**, *94*, 635–650. [CrossRef]
8. Nesbitt, H.W.; Young, G.M. Early Proterozoic climates and plate motions inferred from major element chemistry of lutites. *Nature* **1982**, *299*, 715–717. [CrossRef]
9. McLennan, S.M.; Hemming, S.; McDaniel, D.K.; Hanson, G.N. Geochemical approaches to sedimentation, provenance, and tectonics. *Geol. Soc. Am.* **1993**, *284*, 21–40.
10. Critelli, S.; Le Pera, E.; Ingersoll, R.V. The effect of source lithology, transport, deposition and sampling scale on the composition of southern California sand. *Sedimentology* **1997**, *44*, 653–671. [CrossRef]
11. Ingersoll, R.V. Actualistic sandstone petrofacies: Discriminating modern and ancient source rocks. *Geology* **1990**, *18*, 733–736. [CrossRef]
12. Huntsman-Mapila, P.; Tiercelin, J.J.; Benoit, M.; Ringrose, S.; Diskin, S.; Cotten, J.; Hémond, C. Sediment geochemistry and tectonic setting: Application of discrimination diagrams to early stages of intracontinental rift evolution, with examples from the Okavango and Southern Tanganyika rift basins. *J. Afr. Earth Sci.* **2009**, *53*, 33–44. [CrossRef]
13. Sarki Yandoka, B.M.; Abdullah, W.H.; Abubakar, M.B.; Hakimi, M.H.; Adegoke, A.K. Geochemical characterisation of Early Cretaceous lacustrine sediments of Bima Formation, Yola Sub-basin, Northern Benue Trough, NE Nigeria: Organic matter input, preservation, paleoenvironment and palaeoclimatic conditions. *Mar. Pet. Geol.* **2015**, *61*, 82–94. [CrossRef]
14. Kotlia, B.S.; Joshi, L.M. Late Holocene climatic changes in Garhwal Himalaya. *Curr. Sci.* **2013**, *104*, 911–919.
15. Rashid, S.A.; Ganai, J.A.; Masoodi, A.; Khan, F.A. Major and trace element geochemistry of lake sediments, India: Implications for weathering and climate control. *Arab. J. Geosci.* **2014**, *8*, 5677–5684. [CrossRef]
16. Ryan, K.M.; Williams, D.M. Testing the reliability of discrimination diagrams for determining the tectonic depositional environment of ancient sedimentary basins. *Chem. Geol.* **2007**, *242*, 103–125. [CrossRef]
17. Nesbitt, H.W.; Young, G.M.; McLennan, S.M.; Keays, R.R. Effects of chemical weathering and sorting on the petrogenesis of siliciclastic sediments, with implications for provenance studies. *J. Geol.* **1996**, *104*, 525–542. [CrossRef]
18. Ohta, T. Measuring and adjusting the weathering and hydraulic sorting effects for rigorous provenance analysis of sedimentary rocks: A case study from the Jurassic Ashikita Group, south-west Japan. *Sedimentology* **2008**, *55*, 1687–1701. [CrossRef]
19. Cheong, C.H.; Kim, G.S. *The Geological Map of Neungju Sheet (1:50,000) and Explanatory Text*; Geological Survey of Korea: Daejeon, Korea, 1966; p. 42. (In Korean and English)
20. Kim, B.K.; Park, B.K. *The Geological Map of Dongbok Sheet (1:50,000) and Explanatory Text*; Geological Survey of Korea: Daejeon, Korea, 1966; p. 33. (In Korean and English)
21. Kim, K.B.; Lee, B.J.; Hwang, S.K. *The Geological Map of Kwangju Sheet (1:50,000) and Geological Report*; Korea Institute of Energy and Resources: Daejeon, Korea, 1990; p. 20. (In Korean and English)
22. Son, C.M.; Kim, S.J. *The Geological Map of Changpyeong Sheet (1:50,000) and Explanatory Text*; Geological Survey of Korea: Daejeon, Korea, 1966; p. 30. (In Korean and English)
23. Choi, Y.K.; Yoon, H.D. *The Geological Map of Jangheung Sheet (1:50,000) and Explanatory Text*; Geological Survey of Korea: Daejeon, Korea, 1968; p. 18. (In Korean and English)
24. Hong, S.H.; Yun, U. *The Geological Map of Songjong Sheet (1:50,000) and Geological Report*; Korea Institute of Energy and Resources: Daejeon, Korea, 1986; p. 23. (In Korean and English)
25. Lee, S.M.; Kim, H.S. *The Geological Map of Bongnae Sheet (1:50,000) and Explanatory Text*; Geological Survey of Korea: Daejeon, Korea, 1966; p. 44. (in Korean and English)

26. Lee, H.; Sim, M.S.; Choi, T. Stratigraphic evolution of the northern part of the Cretaceous Neungju Basin, South Korea. *Geosci. J.* **2019**, *23*, 849–865. [CrossRef]
27. Chun, S.S.; Chough, S.K. Tectonic history of Cretaceous sedimentary basins in the southwestern Korean Peninsula and Yellow Sea. In *Sedimentary Basins in the Korean Peninsula and Adjacent Seas*; Chough, S.K., Ed.; Korean Sedimentology Research Group: Seoul, Korea, 1992; pp. 60–76, Special Publication 1.
28. Chough, S.K.; Kwon, S.T.; Ree, J.H.; Choi, D.K. Tectonic and sedimentary evolution of the Korea peninsula: A review and new view. *Earth Sci. Rev.* **2000**, *52*, 175–235. [CrossRef]
29. Wu, F.Y.; Han, R.H.; Yang, J.H.; Wilde, S.A.; Zhai, M.G.; Park, S.C. Initial constraints on the timing of granitic magmatism in North Korea using U–Pb zircon geochronology. *Chem. Geol.* **2007**, *238*, 232–248. [CrossRef]
30. Ahn, K.S.; Huh, M.; Son, J.M. Geological history and landscape of Mudeungsan National Park. *J. Geol. Soc. Korea* **2014**, *50*, 91–105. [CrossRef]
31. Turek, A.; Kim, C.B. U-Pb zircon ages of Mesozoic plutons in the Damyang–Geochang area, Ryongnam massif, Korea. *Geochem. J.* **1995**, *29*, 243–258. [CrossRef]
32. Seo, H.G.; Paik, S.H. *Researches on Coal Resources (II), North Part of the Iyang Area, Honam Coal Field, 83-Coal Resources-3-16*; Geological Survey of Korea: Daejeon, Korea, 1984. (In Korean)
33. You, H.S.; Moon, B.C.; Koh, Y.K.; Kim, H.G.; Lyu, S.O. A study on the paleodepositional environment of Cretaceous sedimentary rocks—Northeastern area of Chonnam. *J. Korean Earth Sci. Soc.* **1998**, *19*, 318–328.
34. Paik, I.S.; Huh, M.; So, Y.H.; Lee, J.E.; Kim, H.J. Traces of evaporites in Upper Cretaceous lacustrine deposits of Korea: Origin and paleoenvironmental implications. *J. Asian Earth Sci.* **2007**, *30*, 93–107. [CrossRef]
35. Wiedenbeck, M.; Alle, P.; Corfu, F.; Griffin, W.L.; Meier, M.; Oberli, F.; von Quadt, A.; Roddick, J.C.; Spiegel, W. Three natural zircon standards for U-Th-Pb, Lu-Hf, trace element and REE analyses. *Geostand. Geoanal. Res.* **1995**, *19*, 1–23. [CrossRef]
36. Andersen, T. Correction of common lead in U-Pb analyses that do not report ^{204}Pb. *Chem. Geol.* **2002**, *192*, 59–79. [CrossRef]
37. Paton, C.; Hellstrom, J.; Paul, B.; Woodhead, J.D.; Hergt, J. Iolite: Freeware for the visualization and processing of mass spectrometric data. *J. Anal. Atom. Spectrom.* **2011**, *26*, 2508–2518. [CrossRef]
38. Paton, C.; Woodhead, J.D.; Hellstrom, J.C.; Hergt, J.M.; Greig, A.; Maas, R. Improved laser ablation U-Pb zircon geochronology through robust downhole fractionation correction. *Geochem. Geophy. Geosyst.* **2010**, *11*, Q0AA06. [CrossRef]
39. Ludwig, K.R. *User's Manual for Isoplot 3.6: A Geochronological Toolkit for Microsoft Excel*; Berkeley Geochronology Center Special Publication: Berkeley, CA, USA, 2008.
40. Taylor, S.R.; McLennan, S.M. *The Continental Crust: Its Composition and Evolution*; Blackwell Scientific Publications: Oxford, UK, 1985; p. 315.
41. Verma, S.P.; Armstrong-Altrin, J.S. New multi-dimensional diagrams for tectonic discrimination of siliciclastic sediments and their application to Precambrian basins. *Chem. Geol.* **2013**, *355*, 117–133. [CrossRef]
42. Fedo, C.M.; Nesbitt, H.W.; Young, G.M. Unraveling the effects of potassium metasomatism in sedimentary rocks and paleosols, with implications for paleoweathering conditions and provenance. *Geology* **1995**, *23*, 921–924. [CrossRef]
43. Buggle, B.; Glaser, B.; Hambach, U.; Gerasimenko, N.; Marković, S. An evaluation of geochemical weathering indices in loess–paleosol studies. *Quat. Int.* **2011**, *240*, 12–21. [CrossRef]
44. Vogt, T. Sulitjelmafeltets geologi og petrografi. *Nor. Geol. Unders.* **1927**, *121*, 1–560. (In Norwegian with English abstract)
45. Parker, A. An index of weathering for silicate rocks. *Geol. Mag.* **1970**, *107*, 501–504. [CrossRef]
46. Jayawardena, U.D.S.; Izawa, E. A new chemical index of weathering for metamorphic silicate rocks in tropical regions: A study from Sri Lanka. *Eng. Geol.* **1994**, *36*, 303–310. [CrossRef]
47. Kim, S.W.; Kwon, S.; Park, S.I.; Lee, C.; Cho, D.L.; Lee, H.J.; Ko, K.; Kim, S.J. SHRIMP U–Pb dating and geochemistry of the Cretaceous plutonic rocks in the Korean Peninsula: A new tectonic model of the Cretaceous Korean Peninsula. *Lithos* **2016**, *262*, 88–106. [CrossRef]
48. Kwon, C.W.; Ko, K.; Gihm, Y.S.; Koh, H.J.; Kim, H. Late Cretaceous volcanic arc system in southwest Korea: Distribution, lithology, age, and tectonic implications. *Cretac. Res.* **2017**, *75*, 125–140. [CrossRef]
49. Gastil, R.G. The distribution of mineral dates in time and space. *Am. J. Sci.* **1960**, *258*, 1–35. [CrossRef]
50. Condie, K.C. Episodic continental growth and supercontinents: A mantle avalanche connection? *Earth Planet. Sci. Lett.* **1998**, *163*, 97–108. [CrossRef]

51. Kim, J.; Cho, M. Low-pressure metamorphism and leucogranite magmatism, northeastern Yeongnam Massif, Korea: Implication for Paleoproterozoic crustal evolution. *Precambrian Res.* **2003**, *122*, 235–251. [CrossRef]
52. Lee, Y.I.; Choi, T.; Orihashi, Y. LA-ICP-MS zircon U-Pb ages of the Precambrian Yuli Group. *J. Geol. Soc. Korea* **2011**, *47*, 81–87. (In Korean with English abstract)
53. Choi, T.; Lee, Y.I.; Orihashi, Y. Crustal growth history of the Korean Peninsula: Constraints from detrital zircon ages in modern river sediments. *Geosci. Front.* **2016**, *7*, 704–714.
54. Park, Y.J. SHRIMP U-Pb Age Distribution of the Detrital Zircons from the Sedimentary and Metasedimentary Rocks of the Southwestern Part of the Korean Peninsula. Master's Thesis, Pukyong National University, Busan, Korea, 2013. (In Korean with English abstract)
55. Nakayama, K.; Yoshikawa, S. Depositional processes of primary to reworked volcaniclastics on an alluvial plain; an example from the Lower Pliocene Ohta tephra bed of the Tokai Group, central Japan. *Sediment. Geol.* **1997**, *107*, 211–229.
56. Ashley, G.M.; Hay, R.L. Sedimentation patterns in a Plio-Pleistocene volcaniclastic rift-platform basin, Olduvai Gorge, Tanzania. In *Sedimentation in Continental Rifts*; Renaut, R.W., Ashley, G.M., Eds.; Society for Sedimentary Geology (SEPM): Broken Arrow, OK, USA, 2002. [CrossRef]
57. Lee, S.G.; Kim, D.Y. Geochemical composition of the continental crust in Korean Peninsula. *J. Pet. Soc. Korea* **2012**, *21*, 113–128. (In Korean with English abstract)
58. Koh, J.S.; Yun, S.H.; Kim, Y.L. Petrology of the Mt. Dungjuribong Volcanic Complex, Gurye-gun, southwest of Ryeongnam Massif. *J. Pet. Soc. Korea* **2009**, *18*, 349–370. (In Korean and English abstract)
59. Kim, Y.L.; Koh, J.S.; Lee, J.H.; Yun, S.H. Petrological study on the Cretaceous volcanic rocks in the southwest Ryeongnam Massif: (1) the Mt. Moonyu volcanic mass, Seungju-gun. *J. Pet. Soc. Korea* **2008**, *17*, 57–82. (In Korean with English abstract)
60. Jung, W.; Ki, Y.; Huh, M. A petrological study of the Mudeungsan Tuff focused on Cheonwangbong and Anyangsan. *J. Pet. Soc. Korea* **2014**, *23*, 325–336. (In Korean and English abstract)
61. Huh, M.; Paik, I.S.; Lockley, M.G.; Hwang, K.G.; Kim, B.S.; Kwak, S.K. Well-preserved theropod tracks from the Upper Cretaceous of Hwasun County, southwestern South Korea, and their paleobiological implications. *Cretac. Res.* **2006**, *27*, 123–138. [CrossRef]
62. Paik, I.S.; Lee, Y.I.; Kim, H.J.; Huh, M. Time, Space and Structure on the Korea Cretaceous Dinosaur Coast: Cretaceous Stratigraphy, Geochronology, and Paleoenvironments. *Ichnos* **2012**, *19*, 6–16. [CrossRef]
63. Lee, J.I.; Lee, Y.I. Geochemistry and provenance of Lower Cretaceous Sindong and Hayang mudrocks, Gyeongsang Basin, southeastern Korea. *Geosci. J.* **2003**, *7*, 107–122.
64. Nesbitt, H.W.; Fedo, C.M.; Young, G.M. Quartz and feldspar stability, steady and non-steady-state weathering, and petrogenesis of siliciclastic sands and muds. *J. Geol.* **1997**, *105*, 173–191. [CrossRef]
65. Lee, Y.I. Geochemistry of shales of the Upper Cretaceous Hayang Group, SE Korea: Implications for provenance and source weathering at an active continental margin. *Sediment. Geol.* **2009**, *215*, 1–12. [CrossRef]
66. Joo, Y.J.; Elwood Madden, M.E.; Soreghan, G.S. Anomalously low chemical weathering in fluvial sediment of a tropical watershed (Puerto Rico). *Geology* **2018**, *46*, 691–694. [CrossRef]
67. Smith, G.A. Facies sequences and geometries in continental volcaniclastic sediments. In *Sedimentation in Volcanic Settings*; Fisher, R.V., Smith, G.A., Eds.; Society for Sedimentary Geology (SEPM): Broken Arrow, OK, USA, 1991.
68. Smith, G.A. Sedimentology of proximal and distal volcaniclastics dispersed across an active foldbelt: Ellensburg Formation (late Miocene), central Washington. *Sedimentology* **1988**, *35*, 953–977. [CrossRef]